Direct-write fabrication of freestanding nanocomposite strain sensors

Rouhollah Dermanaki Farahani[1], Hamid Dalir[1], Vincent Le Borgne[2], Loick. A. Gautier[2], My Ali El Khakani[2], Martin Lévesque[1], and Daniel Therriault[1]*

[1]Laboratory for Multiscale Mechanics, Center for applied research on polymers (CREPEC), École Polytechnique de Montreal, C.P. 6079, succ. Centre-Ville, Montreal (QC), H3C 3A7 (Canada)
E-mail: daniel.therriault@polymtl.ca

[2]Institut National de la Recherche Scientifique, INRS-Énergie, Matériaux et Télécommunications, 1650 Blvd. Lionel-Boulet, Varennes (QC), J3X 1S2 (Canada)

Abstract

This paper deals with the design and microfabrication of two three-dimensional (3D) freestanding patterned strain sensors made of single-walled carbon nanotubes (SWCNTs) nanocomposites with the ultraviolet-assisted direct-write (UV-DW) technique. The first sensor consisted of three nanocomposite microfibers suspended between two rectangular epoxy pads. The flexibility of the UV-DW technique enables manufacturing the sensor and its housing in one monolithic structure. The second sensor was composed of a nanocomposite network consisting of four parallel microsprings, which demonstrates the high capability of the technique when compared to the conventional photolithographic technologies. The performances of the sensors were assessed under tension and compression, respectively. The sensors sensitivities were evaluated by correlating their measured resistivities to the applied displacements/strains. Electrical conductivity measurements revealed that the manufactured sensors are highly sensitive to small mechanical disturbances, especially for lower nanotube loadings when compared to traditional metallic or nanocomposite films. The present manufacturing method offers a new perspective for manufacturing highly sensitive 3D freestanding microstructured sensors.

1. Introduction

There has been a growing interest over the past decade for the development of carbon nanotubes (CNTs)-reinforced polymer nanocomposites, considered as realistic alternatives to conventional smart materials [1-11]. CNTs high aspect ratio [12] and excellent electrical properties [13] confer electrical conductivity and sensing capability to inherently insulating polymers, which make their nanocomposites suitable for use in a broad range of potential applications such as electrostatic charge protection for aircrafts [14], sensors [2,8,10,11], actuators [1,15] and electromagnetic interference shielding [10,14].

Among these applications, CNTs-reinforced polymer nanocomposite films have been extensively used for structural health monitoring for industrial and national infrastructures [4,5,8]. Nanocomposite films strain sensors might be preferred over conventional metal foil strain sensors in some applications due to their enhanced electromechanical sensitivity and their ability to accurately measure large strains [16]. Nanocomposite sensors' electromechanical sensitivity stems from the rearrangement of percolating conducting pathways induced by an external mechanical disturbance. In particular, the nanocomposite films electrical conductivity decreases with increasing mechanical strain under tension because the distances between non-contacting neighboring nanotubes are increased and/or the contact area between the nanotubes in their percolation pathways are influenced [3]. Another possible contribution may arise from the intrinsic CNTs conductivity variation due to mechanical strain, as reported in the literature [17-19]. It has been found that nanotubes concentration, dispersion and manufacturing process are the key parameters affecting the electromechanical sensitivity of such nanocomposite-based sensors. In general, the highest sensitivity is achieved when the nanotubes contents approaches the percolation concentration threshold where the electron tunneling between the neighboring nanotubes at sufficiently close proximity is the dominant mechanism [3].

Most of the researches have been limited to the use of nanocomposite films to manufacture strain sensors [5,10,17-19]. Nanocomposite films are limited, by nature, to only provide in-plane strain measurements. In addition, they must be bonded over their whole area and might capture undesired parasitic perturbations (local cracks, plasticity, etc.) in applications where overall measurements are sought. The sensitivity of such sensors can be improved by decreasing their width and thickness [20]. However, this potential tailoring is somewhat limited by fabrication and manipulation constraints. Finally, bulk nanocomposite films cannot be patterned as traditional strain sensors consisting of a long, thin conductive strip of patterned lines. This limits further the possibilities for improving their sensitivities. Photolithography techniques (resolution down to 120 nm [21]) could be used for manufacturing patterned nanocomposite strain sensors. This technique could also enable to fabricate sensing elements directly on structures surfaces [22]. However, this technique is far from being cost-effective. Therefore, new advances on the fabrication processes are still needed to easily and cost-effectively manufacture a supported or freestanding nanocomposite strain sensor with desired 2D and 3D patterns.

This paper focuses on the use of the ultraviolet-assisted direct-write (UV-DW) technique recently developed in our group [23] for the fabrication of freestanding nanocomposite patterned strain sensors. The flexibility of this fabrication method enabled to tailor and cost-effectively pattern deposited nanocomposite 2D lines like traditional strain gauges and also to fabricate two freestanding 3D-patterned strain sensors. The first manufactured freestanding strain sensor consisted of three nanocomposite microfibers suspended between two rectangular epoxy pads. The electromechanical sensitivity of the structure was evaluated under tensile loading in a dynamic mechanical analyzer (DMA) with a film tension clamp. The second sensor was composed of a square network of four parallel microsprings enclosed by two circular pads at its top and bottom. The sensitivity of this sensor was characterized in DMA with a compression clamp. The

manufacturing technique presented here opens new prospects for the achievement of cost-effective geometry-optimized nanocomposite microdevices for microelectronics applications.

The paper is organized as follows: Section 2 deals with all the experimental details including nanotube characterization with a few methods, nanocomposites preparation procedure and their viscosity characterization. This is followed by the fabrication of two freestanding nanocomposite patterned strain sensors with the UV-DW technique. All the results obtained from the experiments are discussed in section 3. This section begins with the CNTs and their epoxy nanocomposites viscosity characterization. Finally, the nanocomposite sensors electromechanical sensitivities are presented and discussed.

2. Experimental Details

2.1. Nanocomposite preparation and characterization

The SWCNTs were synthesized by the UV-laser ablation (248 nm, 20 ns, 400 mJ) method using a Co/Ni-doped graphite target in an argon atmosphere at a temperature of 1150°C. The as-produced SWCNTs were then subjected to a three-step chemical purification treatment (details can be found in [24,25]) to remove the impurities like metal catalyst particles and other carbonaceous structures.

The purified SWCNTs were then used to prepare nanocomposites at different nanotube loadings by mixing them with an ultraviolet/heat curable epoxy (UV-epoxy, UV15DC80, Master Bond Inc.). The UV-epoxy used here contains a UV photo-initiator with an optimal absorption at 365 nm and a heat-initiator active in the 60 - 80°C range. Nanotubes non-covalent functionalization using surfactant was applied to the nanotube aggregates solubilization. The desired amount of purified SWCNTs was added to a solution of 0.1 mM of Zinc protoporphyrin IX (Sigma-Aldrich) in acetone. The suspension was sonicated in an ultrasonic bath (Ultrasonic cleaner 8891, Cole-Parmer) for 90 min. The UV-epoxy was then slowly mixed with the nanotube suspension in acetone over a

magnetic stirring hot plate (Model SP131825, Barnstead international) at 50°C for 4 h. The solvent was evaporated by placing the nanocomposite under hood at room temperature for 24 h, followed vacuumed-oven (RK-52402, Cole Parmer) curing at 30°C for 12 h and at 50°C for 24 h. The nanocomposites were passed through a three-roll mill mixer (Exakt 80E, Exakt Technologies) for final high shear mixing upon solvent evaporation. The gaps between the rolls varied in three batch-wise processing steps including 5 passes at 25 µm, 5 passes at 10 µm and 10 passes at 5 µm, respectively. The rotation speed of the apron roll was set to 250 RPM. The final mixture was then degassed under a vacuum of 0.15 bar for 24 h.

The purified SWCNTs were observed by transmission electron microscopy (TEM) using a Jeol JEM-2100F (FEG-TEM, 200 kV) microscope. Their Raman spectra were acquired at room temperature in the 100 - 2000 cm^{-1} spectral region under ambient conditions using a back-scattering geometry on a microRaman microscope (Renishaw Imaging Microscope Wire TM) with a 50× objective. A 514.5 nm (2.41 eV) line from an air cooled Ar+ laser was used for excitation radiation.

The process-related apparent viscosity of the pure UV-epoxy and its associated nanocomposites were measured from an experimental method based on capillary viscometry [26,27]. To obtain different shear conditions, ten continuous filaments of materials were extruded through a micro-nozzle (5132-0.25-B, Precision Stainless Steel Tips, EFD, L = ~20 mm and Internal Diameter (ID) = 100 µm) at five different pressures over glass substrates. The filaments were deposited using a computer-controlled robot (I & J2200-4, I & J Fisnar) and a fluid dispenser (HP-7X, EFD) with a calibrated deposition speed. Shortly after the deposition, the filaments were cured under a UV lamp (RK-97600, Cole-Parmer) illumination for 5 min. The materials flow rates were calculated from the filaments cross-section and the extrusion speed was controlled by the dispensing apparatus. The cross-section area of the filaments was measured with an optical microscope (BX-61, Olympus) and image analysis software (Image-Pro Plus V5, Media Cybernetics). The process-related apparent

viscosity and the process-related apparent shear rate were calculated from capillary viscometry equations including Rabinowitsch correction.

2.2. Fabrication of the sensors and their characterizations

UV-DW technique was used to fabricate nanocomposite-based strain sensors. The UV-DW technique relies on a computer-controlled robot (I & J2200-4, I & J Fisnar) that moves a dispensing apparatus (HP-7X, EFD) and a UV light-emission set-up along the *x*, *y* and *z* axes. Figure 1a schematically represents the fabrication of different microstructures using UV-curable nanocomposite materials. The materials are photopolymerized under the illumination of UV light using two high-intensity UV light-emitting diodes (LED, NCSU033A, Nichia) while being extruded. The fast-curing of nanocomposite materials enables the fabrication of supported or freestanding 3D structures when the extrusion position spatially changes in three dimensions. Figures 1b and 1c show optical images of two deposited nanocomposite microstructures with a sufficient control of the resolution and patterns manufactured with this flexible, efficient and cost-effective method. In particular, the network shown in Figure 1b was fabricated in only 20 seconds.

The UV-DW technique was also used to fabricate two 3D-patternned freestanding nanocomposite strain sensors. In the first sensor, three 100µm-diameter nanocomposite microfibers suspended over a 8 mm gap between two rectangular epoxy pads were fabricated by extruding the nanocomposites suspension through a micro-nozzle (Precision Stainless Steel Tips, EFD, internal diameter = 100 µm). The two epoxy pads were silver-coated for ensuring proper electrical contact and served as electrodes. Another layer of epoxy was subsequently deposited over the two pads using the UV-DW technique. This insulated electrically the fibers in order to reduce the parasitic effects.

The second type of sensors was composed of a square network of four identical 1mm-diameter microsprings. The microsprings were fabricated on a small circular aluminum plate in a rectangular

layout having an inter-coil distance of 2 mm. Another aluminum plate was subsequently attached to the top of the springs. Eelectrical measurement probes were attached to the aluminum plates which served as conductive electrodes. Finally, the microfibers and the microspring networks were post-cured at 120°C for 1 h.

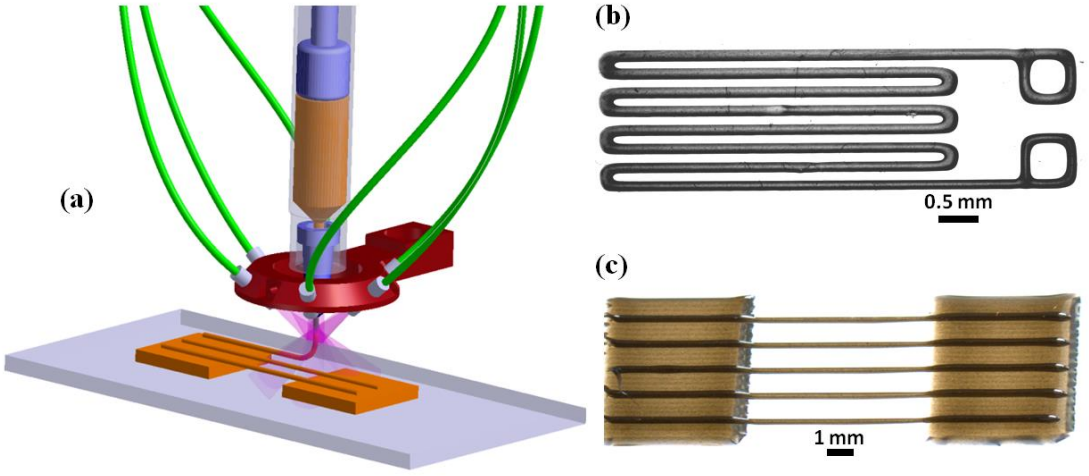

Figure 1. (a) Schematic representation of the UV-assisted direct-writing of nanocomposite microstructures, (b) a deposited line network similar to traditional strain gauges and (c) a microfibers coupon. To fabricate these microstructures using the UV-DW technique, the nanocomposite is extruded through a capillary micronozzle by an applied pressure and is partially cured shortly after extrusion under UV illumination.

The sensors electromechanical sensitivity was evaluated by relating both their measured electrical conductivity and strains (or displacements) as the sensors underwent mechanical loading. The nanocomposite-based sensors electrical conductivities were measured with a Keithley 4200 semiconductor parametric analyzer (MM 2000 probe station). The strain sensors mechanical response (i.e., force–displacement) was measured in a dynamic mechanical analyzer (DMA, DMA2980, TA instruments). The microfibers were tested using a film tension clamp with a constant loading rate of 0.5 N/min^{-2} to reach a maximum displacement of 1 mm. The microsprings network mechanical response under compression was characterized with a compression fixture at a load rate of 5 mN/min^{-2} for a maximum displacement of 3 mm.

3. Results and discussions

3.1. Carbon nanotube characterization

Figure 2a shows a typical laser-synthesized SWCNTs TEM micrograph after their chemical purification. The nanotubes are observed to self-organize into high aspect ratio (i.e., length/diameter) bundles (length: up to 10 µm; diameter: ~1.24 nm). The nanotube chemical purification removed any residual catalyst particles and other carbonaceous structures. However, few dark spots are still observed. These are most probably residual catalyst nanoparticles that were not entirely digested during the nitric acid oxidation treatment.

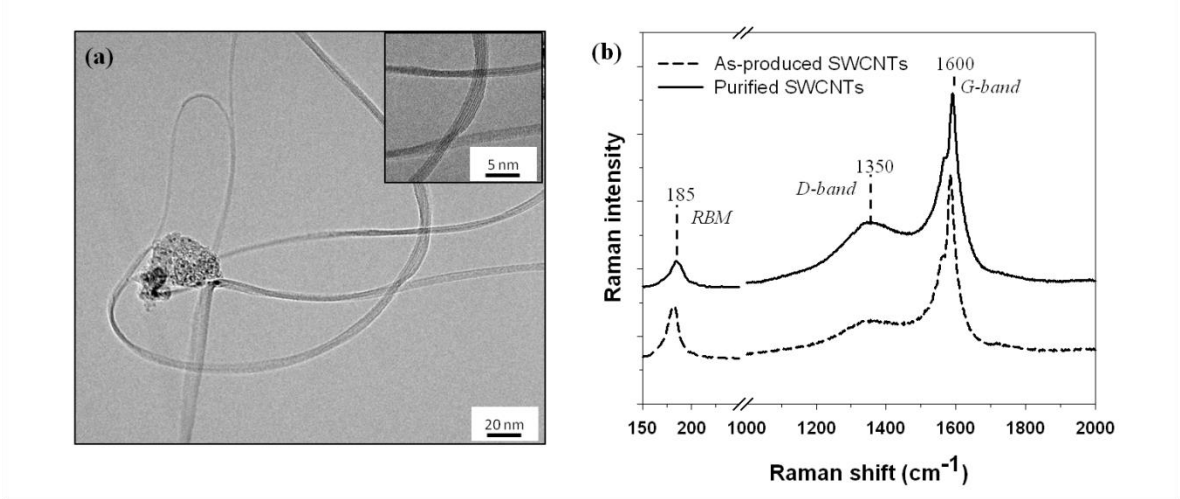

Figure 2. (a) Typical TEM images of purified SWCNTs and (b) Raman spectra as-produced (bottom) and purified (top) SWCNTs.

The structure of as-produced and purified SWCNTs was characterized using Raman spectroscopy. Figure 2b shows typical Raman spectra of the as-produced and purified SWCNTs, representing three typical peaks for the carbon nanotubes. The spectra includes a narrow radial breathing mode (*RBM*) band centered around 185 cm^{-1}, the *D*-band centered around 1350 cm^{-1} and the *G*-band around 1600 cm^{-1}. The RBM peak is attributed to the presence of SWCNTs with a mean diameter of 1.2 nm, in accordance with the measurements from direct TEM observations. The *G*-band corresponds to the symmetric vibrational tangential mode in graphite-like materials and the *D*-

band is as a signature of disorder and/or defects in these structures. The high *G/D* intensity ratio is generally used to qualify the nanotubes purity. When the nanotubes were subjected to the purification process, their *G/D* intensity ratio significantly decreased in comparison to that of the as-produced mats. This is a consequence of the creation of additional structural defects in the nanotubes surface during the nitric acid oxidation based purification process. However, the improved dispersion enabled by the creation of functional groups during the purification process outweighs their drawbacks with respect to nanotube conductivity [28].

3.2. Nanocomposite viscosity characterization

Materials viscosity is a critical parameter in the UV-DW technique. Extruded materials of moderate to high viscosities are necessary to create stable filaments [23, 27]. Since high viscosity may limit flow through fine extrusion nozzles, an extruded materials shear-thinning behavior (i.e., a decrease of viscosity with an increase of shear forces inside the nozzle) is preferable. Figure 3 shows the process-related apparent viscosity (η_{app}) with respect to the process-related apparent shear rates ($\dot{\gamma}_{app}$) induced by the extrusion of the neat UV-epoxy and its associated nanocomposites for five extrusion pressures. A nearly constant η_{app} of ~12 Pa.s is observed for the neat UV-epoxy, indicating a Newtonian behavior in the range of shear rates studied. The incorporation of purified SWCNTs to the neat resin resulted in a considerable increase (12-fold increase by adding 1 wt% SWCNTs) for η_{app} at low $\dot{\gamma}_{app}$ and the apparition of a shear-thinning behavior. The carbon nanotubes high aspect ratio which possibly enabled the formation of a rheological percolation network and also their possible orientation during extrusion is thought to be responsible for the observed shear thinning behavior [29]. The nanocomposites viscosity and shear thinning behavior enabled the fabrication of microfibers coupons as well as the microsprings networks with the UV-DW technique.

The nanocomposites viscosity increase is also a good indicator for the nanotubes dispersion quality [30]. This is also supported by optical and SEM observation [31]. The achieved dispersion is the result of nanocomposite mixture ultrasonication combined with important shear forces induced in the three-roll mixer.

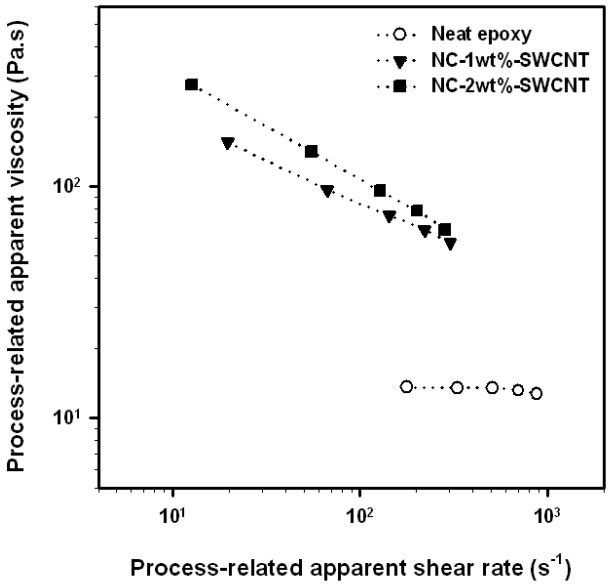

Figure 3. Process-related apparent viscosity of the neat UV-epoxy and its nanocomposites with respect to apparent shear rate using a method based on capillary viscometry.

3.3. Sensors electromechanical sensitivity

3.3.1. Microfibers coupon

Figure 4 presents various aspects related to the nanocomposite microfibers coupons electromechanical testing. Figure 4a shows a typical microfibers optical image. Figure 4b shows that the freestanding microfibers circular cross-section with a diameter of ~ 120 µm. To avoid the microfibers failure during the electromechanical testing, the displacement at break was measured that is found to be ~ 1.5 mm (corresponds to ~ 0.19 of tensile strain). Therefore, the tensile testing was stopped when the displacement reached to a maximum of 1 mm. Figure 4c shows the force–displacement curves obtained for the nanocomposite microfibers for the range of displacements

studied (average on five specimens for each fiber type). The nanocomposite microfibers for both nanotube loadings exhibit a non-linear response. This behavior might be due to the possible toughening effect of the nanotubes [32] since the response of neat epoxy resins is linearly elastic. The rigidity (i.e., tangent of curves in their linear parts) of the nanocomposite microfibers containing 1 wt% SWCNTs was found to be ~ 4.7 N mm^{-1}, and increased to ~ 6.3 N mm^{-1} (about 34% increase) for the fibers reinforced with 2 wt% SWCNTs. This might be attributed to the potentially high elasticity of SWCNTs, their proper dispersion and their possible beneficial orientation that may occur during the extrusion of the nanocomposite through the micronozzle.

Figures 4d and 4e show the current with respect to applied voltage (I-V) curves for the nanocomposite microfibers measured at three different strains and for nanotube loadings of 1 wt% and 2 wt%, respectively. Table 1 lists the microfibers electrical conductivities for five different strains. Nearly linear responses were observed for all nanocomposite microfibers within the voltage range investigated. The increase of nanotube contents increased the electrical conductivity of the microfibers and also decreased their electromechanical sensitivity, as listed in Table 1. Electromechanical sensitivity is usually represented as gauge factor defined as the ratio of relative resistance variation over strain variation. Higher nanotube loadings enhance the probability of contact points through which electrons are transferred and also decrease the distance of adjacent nanotubes [4,16]. As a result, electrical conductivity is less susceptible to strain at higher nanotube loadings. A large value of the gauge factor was obtained despite the relatively high nanotube concentrations when compared to that of percolation concentration threshold. This might be attributed to the proper nanotubes dispersion of and also the small microfibers diameters since gauge factor is strongly influenced by the nanocomposite geometry. Finally, Figure 4f shows the microfibers resistivity variation as a function of the applied tensile strains. The curves non-linearity might be due to neighboring nanotubes separation through which electron tunneling is compromised [3].

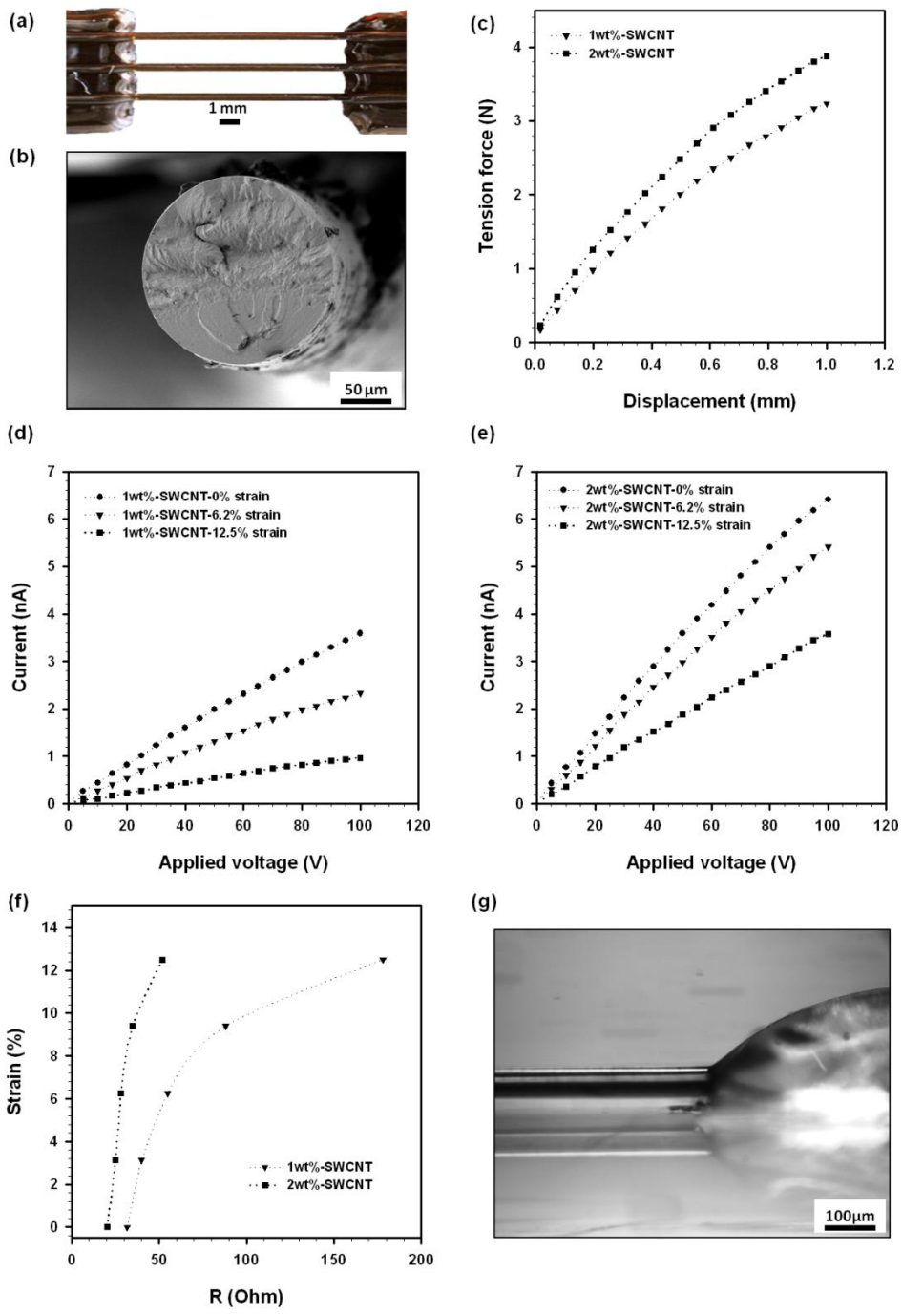

Figure 4. Electromechanical characterization of the nanocomposite microfibers under tensile strains: (a) optical image of a typical fabricated specimen consisting of three suspended fibers between two rectangular pads, (b) SEM image of fracture surface of a nanocomposite fiber, (c) typical force–displacement curves, (d) and (e) measured current upon voltage application between two pads for the nanocomposite microfibers respectively at 1wt% and 2wt% SWCNTs loadings, (f) strain-resistivity correlated curves based on electrical resistivity changes and (g) an optical image of a microfibers coupon adhered to a structure from the pads.

Table 1. Electrical conductivity changes for the microfibers under applied strains.

Electrical conductivity at different strain ($S.cm^{-1}$)						Gauge factor
Strain (%)	0	3.1	6.2	9.4	12.5	
1 wt.% SWCNTs	1.1×10^{-6}	9.4×10^{-7}	7.1×10^{-7}	4.8×10^{-7}	2.8×10^{-7}	~ 22
2 wt.% SWCNTs	2.0×10^{-6}	1.9×10^{-6}	1.7×10^{-6}	1.4×10^{-6}	1.0×10^{-6}	~ 7

The microfibers coupons could be used as real tensile strain sensors. The epoxy adhesive pads enable to attach the sensor to a structure (Figure 4g) while the freestanding geometry eludes any parasitic effects (local buckling) between the two ends. The geometry of the sensor can be easily tailored, depending on the applications to either sense tensile local strains (e.g., short microfibers) or overall strains (e.g., long microfibers like neurons). Diameter and number of the microfibers also can be controlled by the extrusion nozzle and the deposition robot. Interestingly, the sensor can be fabricated directly on the structure using the flexible UV-DW technique. However, the direct deposition of the sensor elements is possible only if the thickness of structures is smaller than 50 mm (i.e., maximum distance between the extrusion nozzle and the deposition platform of the deposition robot). It is worth noting that the microfibers sensor may find other applications such as a force sensor to measure small tension loads.

3.3.2. Microsprings network

Microsprings networks were manufactured with the aim of fabricating a freestanding strain sensor capable of sensing out-of-plane strains. Figure 5 presents various aspects related to the electromechanical testing of the nanocomposite microsprings networks. Figure 5a shows a SEM image of a typical network consisting of four identical springs with five coils. The first and last coils were flat in order to attach the aluminum pads for electromechanical testing. The final sensor geometry is shown in Figure 5b. The springs were arranged in rectangular array for structural

stability. The manufactured springs geometry matched the programmed robot's paths, which shows the high fidelity of the UV-DW fabrication technique. Figure 5c is a representative SEM image of the nanocomposite filament surface. The filament's diameter was ~ 130 μm, which is larger than that of the extrusion nozzle due to material swelling.

Figure 5d shows force–displacement curves achieved for the microsprings networks under compression. The specific rigidity of the networks was increased (by 28%) with the increase of SWCNTs loading to 2 wt%. Similar to the microfibers tensile experiments, the current was measured under applied voltage between two aluminum pads (top and bottom of the network) at seven different displacements as shown in Figures 5e and 5f (only the curves for three displacements are shown) for different nanotube loadings used. Table 2 summarizes the electrical conductivity of the springs for different displacements under compressive loads. As for microfibers, a linear relationship is obtained. The microsprings network electrical conductivity increased under compressive displacements. This might be due to the increased probability for SWCNTs to be in contact, facilitating electron transfer.

Figure 5g shows the microsprings networks electromechanical sensitivity. The results show that gauge factors of 3.1 and 2.2 were obtained for the sensor with 1 wt.% and 2 wt.% nanotube loadings, respectively. These values could be improved by optimizing the number and diameter of coils and the filaments diameter as well as the nanotube concentration. The desired spring geometry could be easily programmed and fabricated using the UV-DW technique. Although this technique enables to fabricate longer springs, this type of sensor cannot be used for large structures because of fabrication limitations. The microsprings network sensor could be used as a potential accurate scale to measure very small weights and find other applications in micro electromechanical systems.

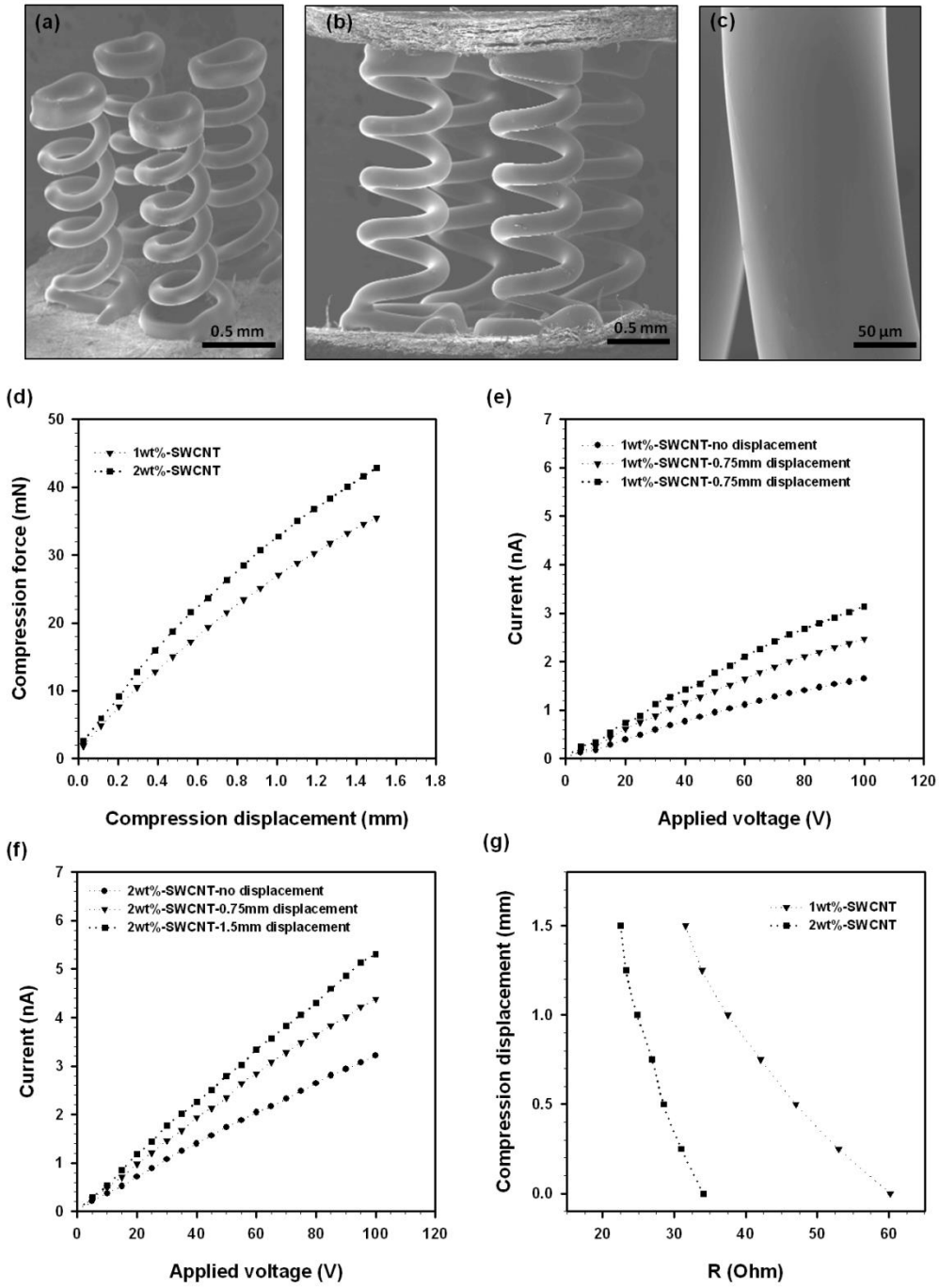

Figure 5. Nanocomposite microsprings electromechanical characterization: (a) SEM image of a typical fabricated specimen consisting of four freestanding microsprings, (b) SEM image of the final configuration of the sensor (a circular pad on the top), (c) filament surface SEM image, (d) typical force–displacement curves, and (e) and (f) measured current upon voltage application between two aluminum pads for the nanocomposite microfibers respectively at 1wt% and 2wt% SWCNTs loadings and (g) displacement-resistivity correlated curves based on electrical resistivity changes for the microsprings network.

Table 2. Electrical conductivity changes for the microsprings network under applied displacements.

Electrical conductivity at different displacements ($S.cm^{-1}$)							
Displacement (mm)	0	0.25	0.5	0.75	1	1.25	1.5
1 wt.% SWCNTs	9.9×10^{-7}	1.0×10^{-6}	1.2×10^{-6}	1.5×10^{-6}	1.6×10^{-7}	1.8×10^{-6}	2.0×10^{-6}
2 wt.% SWCNTs	1.9×10^{-6}	2.0×10^{-6}	2.3×10^{-6}	2.6×10^{-6}	2.8×10^{-6}	3.0×10^{-6}	3.2×10^{-6}

4. Conclusions

Two 3D-patterned freestanding nanocomposite strain sensors were manufactured with UV-DW technique. The nanocomposite-based sensors electromechanical sensitivities were evaluated under tension and compression. A sufficient control of the sensors geometries provided by patterning small-diameter nanocomposite microfibers enabled to reach a fairly-high electromechanical sensitivity (i.e., gauge factor: ~22). Additionally, the results are thought to be more reliable since the freestanding geometry of the sensors may reduce the effect of undesirable stimulus on the results. Higher sensitivity might be achieved at lower nanotube loadings close to their percolation threshold. The contribution of the geometry such as smaller diameter could be easily maximized using the flexible UV-DW technique. Since the strain sensors manufactured here are as examples of 3D MEMS sensors, any other complex pattern for sensing components or other applications in microelectronics such as electromagnetic shielding could be manufactured using this technique.

Acknowledgements

The authors acknowledge the financial support from FQRNT (Le Fonds Québécois de la Recherche sur la Nature et les Technologies). Prof. El Khakani acknowledges also the financial support from NSERC (National Science Engineering Research Council of Canada) and Plasma-Québec (le Réseau Stratégique du FQRNT sur la Science et Technologies des Plasmas). The authors would like to thank the technical support of Dr. B. Aissa from INRS and also Dr. K. Laaziri from

Laboratoire de recherche sur les nanostructures et interfaces conductrices for the electrical measurements.

References

[1] Chou TW, Li C and Thostenson E T 2008 *Compos. Sci. Technol.* **68**, 1227.

[2] Culpepper M L and Cullinan M A 2010 *Phys. Rev. B*. 82, 11.

[3] Hu N, Karube Y, Yan C, Masuda Z and Fukunaga H 2008 *Acta Materialia* **56**, 2929.

[4] Hu N, Yin G, Karube Y, Liu Y L, Li Y and Fukunaga H. 2011 *J. Compos. Mat.* **45**, 1315.

[5] Ji T S, Jung S Y, Xie J N and Varadan V K. 2007 *7th IEEE Conference on Nanotechnology*, **1-3**, 375.

[6] Kchit N and Bossis G. 2009 *J. Phys. D*. **42**.

[7] Kchit N, Lancon P and Bossis G. 2009 *J. Phys. D*. **42**.

[8] Liu Y, Chakrabartty S, Gkinosatis D S, Mohanty A K and Lajnef N. *2007 IEEE Biomedical Circuits and Systems Conference* **119**, 22.

[9] Liu Z M, An G M, Na N, Zhang X R, Miao Z J and Miao S D 2007, *Nanotechnology*, **18**, 435307.

[10] Park Y B, Pham G T, Liang Z, Zhang C, Wang B. 2008, *Composite Part B*, **39**, 209.

[11] Schulte K, Schueler R and Joshi S P. 2001, *Compos. Sci. Technol.* **61**, 921.

[12] Bethune D S, Kiang C H, Devries M S, Gorman G, Savoy R and Vazquez J 1993, *Nature,* **363**, 605.

[13] Tans S J, Devoret M H, Dai H J, Thess A, Smalley R E and Geerligs L J. 1997, *Nature,* **386**, 474.

[14] Baughman R H, Zakhidov A A and de Heer W A. 2002, *Science,* **297**, 787.

[15] Ashrafi B, Hubert P and Vengallatore S. 2006, *Nanotechnology,* **17**, 4895.

[16] Murugaraj P and Mainwaring D. 2011, *Electronic Functionality of Nanocomposites*, **23**, 549.

[17] Singh G, Rice P, Mahajan R L. 2007, *Nanotechnology,* **18**, 47.

[18] Stampfer C, Helbling T, Obergfell D, Schoberle B, Tripp M K and Jungen A. 2006, *Nano Lett.* **6**, 233.

[19] Stampfer C, Jungen A and Hierold C. 2006, *IEEE Sens. J.*, **6**, 613.

[20] Murugaraj P, Mainwaring D E and Mora-Huertas N. 2009, *Compos. Sci. Technol.* **69**, 2454.

[21] Kawata S, Sun H B, Tanaka T and Takada K. 2001, *Nature*, **412**, 697.

[22] Meeusen W, Clijnen J, Reynaerts D, Van Brussel H and Puers R. 2003, *IEEE Sens. J.*, **3**, 632.

[23] Lebel L L, Aissa B, El Khakani M A and Therriault D. 2010, *Adv. Mat.* **22**, 592.

[24] Braidy N, El Khakani M A and Botton G A. 2002, *Carbon*, **40**, 2835.

[25] Le Borgne V, Aissa B, Mohamedi M, Kim Y A, Endo M and El Khakani M A. *J. Nanopart. Res.*DOI: 10.1007/s11051-011-0409-9.

[26] Bruneaux J, Therriault D and Heuzey M C. 2008, *J. Micromech. Microeng.* **18**, 11.

Moniruzzaman M, Du F M, Romero N and Winey K I. 2006, *Polymer*, **47**, 293.

[27] Lebel L L, Aissa B, El Khakani M A and Therriault D. 2010, *Compos. Sci. Technol.* **70**, 518.

[28] Hobbie E K, Obrzut J, Kharchenko S B, Grulke E A. 2006, *J. Chem. Phys.* **125**, 4.

[29] Rahatekar S S, Koziol K K K, Butler S A, Elliott J A, Shaffer M S P, Mackley M R. 2006, *J. Rheol*. **50**, 599.

[30] Thostenson E T, Chou T W. 2006, *Carbon*. **44**, 3022.

[31] Farahani D R, Dalir H, Aissa B, El Khakani M A, Levesque M, Therriault D. 2011, *Composites: Part A.* DOI: 10.1016/j.compositesa.2011.08.016.

[32] Gojny F H, Wichmann M H G, Fiedler B, Schulte K. 2005, *Compos. Sci. Technol.* **65**, 2300.